Journal of Sound and Vibration 369 (2016) 1–15

Contents lists available at ScienceDirect

Journal of Sound and Vibration

journal homepage: www.elsevier.com/locate/jsvi

Flow-induced noise control behind bluff bodies with various leading edges using the surface perturbation technique

Z.B. Lu [a,*], D. Halim [b], L. Cheng [c]

[a] Temasek Laboratories, National University of Singapore, Singapore
[b] Department of Mechanical, Materials and Manufacturing Engineering, The University of Nottingham Ningbo China, China
[c] Department of Mechanical Engineering, The Hong Kong Polytechnic University, Hung Hom, Kowloon, Hong Kong Special Administrative Region

ARTICLE INFO

Article history:
Received 29 April 2015
Received in revised form
11 January 2016
Accepted 16 January 2016
Handling Editor: L. Huang
Available online 2 February 2016

ABSTRACT

The present paper is devoted to an investigation on the flow-induced noise control downstream of bluff bodies with various leading edges using the surface perturbation technique. Four typical leading edges used in various engineering applications were studied in this work: the semi-circular, square, 30° symmetric trapezoid and 30° asymmetric trapezoid leading edges. The surface perturbation was created by piezo-ceramic actuators embedded underneath the surface of a bluff body placed in a cross flow. To suppress the flow-induced noise downstream bluff bodies with those leading edges, the surface perturbation technique was implemented. Based on the experiments, a noise reduction in the duct of more than 14.0 dB has been achieved for all leading-edge cases. These results indicated that the vortex shedding and its flow-induced noise have been successfully suppressed by the proposed control scheme. The flow structure alteration around the bluff bodies and the shear layer shift phenomenon observed on the trailing edges were then investigated for interpreting the control mechanism for this flow-induced noise suppression, which were based on the vortex shedding strength suppression and vortex shedding frequency shift phenomenon. The effective control position for various leading edges was also studied for developing optimal control strategies for practical engineering applications.

1. Introduction

Structural vibration and acoustic noise commonly observed in engineering applications can be caused by the generation of vortex shedding behind a bluff body, which is placed in a cross flow [1–3]. This phenomenon can be classified as one kind of flow–structure–sound (FSS) interaction problems. FSS is relevant to a large variety of applications in mechanical, civil and environmental engineering, thus arousing the extensive research interest during the last few decades. Generally, this phenomenon can be controlled by using either passive or active control methods [4]. Without requiring additional energy input, typical passive control methods include surface modifications with roughness, splitter plate and small secondary control cylinder [5–7]. While in active control methods, the flow system is altered via actuators which are driven by the external energy input. Active control methods can further be classified as open- and closed-loop control depending on

* Corresponding author.
E-mail address: tslluz@nus.edu.sg (Z.B. Lu).

http://dx.doi.org/10.1016/j.jsv.2016.01.028
0022-460X/

whether feedback signals are used in the control process. Rotary, streamwise, transverse oscillations of a bluff body and inflow oscillation [8–11] are the representative open-loop control examples. While typical closed-loop control examples include Berger [12], Huang and Weaver [13], and Cattafesta et al. [14–16] used the feedback signals from the dynamic system for the control actions.

Pursuant to the surface perturbation technique proposed by Cheng et al. [17], a series of experimental studies were carried out using various configurations [18]. It was demonstrated that the actively controlled perturbation could successfully alter the interactions by ensuring proper synchronization between the motion of the perturbed surface and vortex shedding. The primary benefit of this control method is that both vortex shedding strength and the vortex-induced structural vibration could be simultaneously attenuated. The feasibility of using the proposed technique for the control of flow-induced acoustic resonance with downstream acoustic cavities behind a semi-circular leading edge test model was also investigated [19–21]. The latest work [20,21] provided a comprehensive assessment on the efficiency of the technique by using an improved actuator configuration for the semi-circular leading edge bluff body, and more importantly, offered explanations on the control mechanism of the perturbation technique in attenuating the flow-induced sound. It was demonstrated that the effective reduction in the acoustic resonance is originated not only from a direct impairment of the vortex shedding strength, but also from the perturbation-induced vortex shedding frequency shift, that could be predicted using a simple formula, which described that the shift was linearly related to the equivalent increase of the thickness of the bluff body in a flow duct.

However, the exploration on the bluff bodies with either a square leading edge or a semi-circular leading edge are still needed to be generalized for various leading edges so that the surface perturbation technique can be used for various engineering applications. Furthermore, more studies are still required to understand the physical mechanisms of the present control technique on bluff bodies with various leading edges. Thus, bluff bodies with various leading edges were experimentally investigated in the present paper, by using the same technique. Upon control deployment, corresponding flow structure alterations for each test model with different type of leading edge, including the semi-circular, square, 30° symmetric and 30° asymmetric trapezoid leading edge test models were experimentally assessed. Three major objectives in this work are: 1) To assess the performance of the surface perturbation control technique when it is applied to bluff bodies

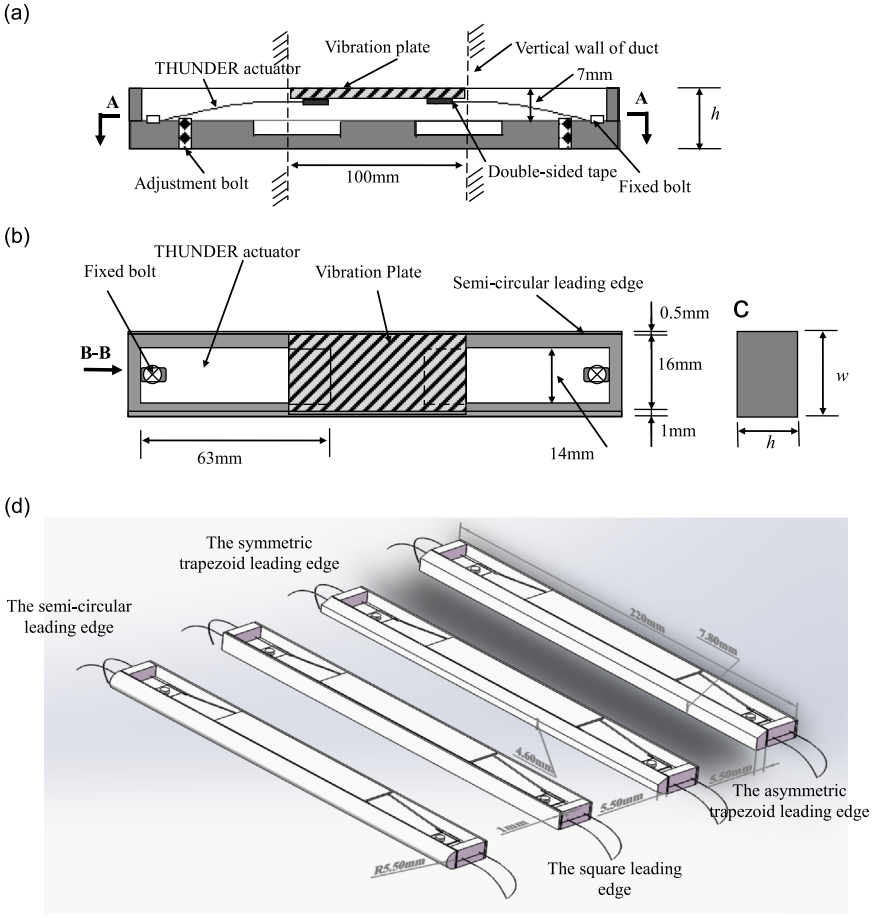

Fig. 1. Test model in details. (a) Installation of the vibration module; (b) Top view A-A of the vibration module; (c) Side view B-B of the vibration module; (d) Various leading edges of the test models in 3D view.

with different leading edges, in both flow and acoustic fields; 2) To document and understand the flow structure alterations around the test model, in terms of the boundary layer structure alteration and its shift from the original position, for further interpreting the mechanism behind the vortex shedding strength suppression and vortex shedding frequency shift phenomenon. 3) To investigate the effective control position for various leading edge test models.

2. Experimental set-up

Measurements were conducted in a closed circuit acoustic wind tunnel (1820 mm-long with a square test section of 100 mm × 100 mm), with details given in the previous work [20], the low background noise was achieved in this wind tunnel since the noise of the motor and fan was mostly absorbed by acoustic duct linings. A rigid thick plate with a zero angle of attack, called the 'test model' in the present experiment, is installed in the flow duct. The two ends of the test model are rigidly fixed on the walls of the duct. THUNDER actuators developed by NASA Langley research center are used in the present experiment for creating relatively large controllable perturbation on the upper surface of the test model.

Details of the test models are shown in Fig. 1. Various leading edges were used in test models (including four typical leading edges commonly used in engineering applications: the semi-circular, square, 30° symmetric trapezoid and 30° asymmetric trapezoid leading edges) with the height of each test model to be $h=11.0$ mm. The length of square leading edge test model was 18.5 mm, while the length of the other test models was 23.0 mm. These test models were made up from a vibration module shown in Fig. 1 and a leading edge module. Two curved THUNDER piezo-ceramic actuators were placed in the test model as shown in Fig. 1. In order to create a maximum displacement in the transverse y-direction, the actuators were installed in a cantilever manner. A thin plastic plate of 1.2 mm thick, called as the 'vibration plate', was mounted flush

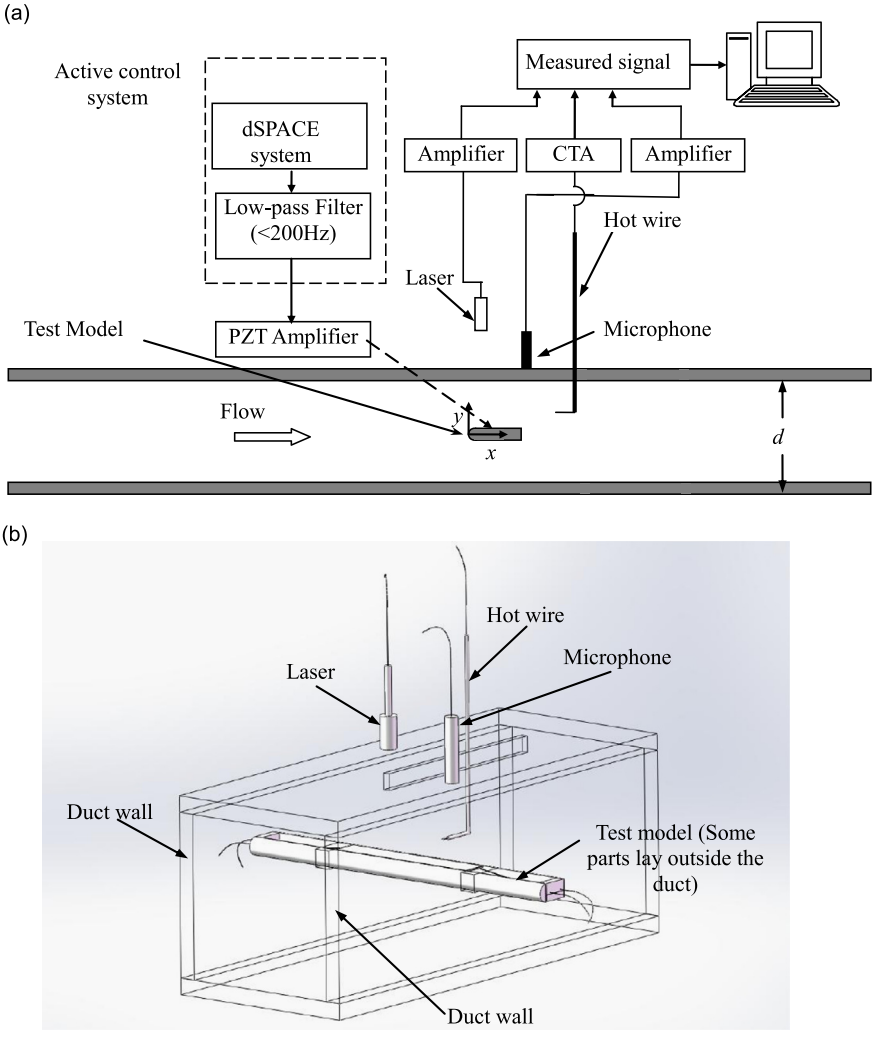

Fig. 2. Experimental setup. (a) Control system and measurement system; (b) Experimental setup in 3D view.

with the upper surface of the plate, and connected with the cantilevered end of the THUNDER actuators by using a double-sided tape. The vibration plate driven by the actuators, would oscillate to create a span-wise uniform transverse vibration along the y-direction of the test model, which were confirmed by the measurement of velocity over the plate using a laser vibrometer. Fig. 1(d) shows the 3D view of the various leading edges of the test models.

Fig. 2 shows the entire test configuration together with the measurement system. To generate the control perturbation, two cantilever actuators were simultaneously activated by a sinusoidal signal with controllable frequency, using the dSPACE rapid control prototyping system, and then amplified by a dual-channel PZT amplifier (Trek PZD 700), as shown in Fig. 2. A sinusoidal signal at a single frequency in an open-loop control scheme was used. The acoustic pressure was measured by a 1/2″ condenser microphone (B&K 4189), which was flush-mounted on the top wall of the duct at the trailing edge of the test models. A 5 μm tungsten single hot wire was deployed to measure the fluctuating flow velocity at various positions around the test model. It could be located at any positions around the test model depending on the requirement of the measurement. Generally, the position of the hotwire was determined in the shear layer or vortex trajectory for measuring the velocity fluctuations to indicate the turbulent region, commonly observed in both before and after control cases. In the present experiment, the flow speed was adjusted in the experiment to ensure that there was stable vortex shedding behind the bluff bodies. Sound is produced when a bluff body placed in the flow fluid [22], later Howe's theory [23] quantified that the sound is associated with periodic shedding of vortices. In a duct, the sound generated is reflected back and can become very loud. When the vortex shedding frequency is close to the frequency of the appropriate acoustic mode in the space, the resonance can occurs over a range of flow velocity [24]. Therefore stable vortex shedding would be generated behind the bluff bodies with a relatively high sound pressure level (SPL) at the vortex shedding frequency. Based on this observation, the experimental set-up, as detailed in this manuscript, was designed to achieve this vortex shedding occurrence. A number of measurements using hot-wire and microphone in the duct have confirmed the existence of vortex shedding behind the bluff body, consistent with the observation from previous works [24,25]. Thus, the subsequent investigations are based on the observation that stable vortex shedding occurred downstream, and the flow velocity fluctuation can be used to identify the vortex shedding strength at the vortex shedding frequency. The hot wire was used to measure velocity fluctuations at the vortex shedding frequency, and these velocity fluctuations assist the identification of the flow structures and their corresponding change around the bluff bodies after the control application. Thus the measured positions of hot wire were determined by the distribution of flow structures around the bluff bodies and the measurement objectives. In addition, a Polytec Series 3000 Dual Beam laser vibrometer was used to measure the displacement at the center of vibrating plate produced by actuators. All measurement signals were recorded for the duration of 11 s using a personal computer through a 12-bit A/D board at a sampling frequency of 6000 Hz per channel after amplification.

In order to have the consistent flow conditions as in the previous work [20,21], the flow velocity was set to the same value $U = 8.2$ m/s. Before the installation of the test model, a single boundary hot wire was used to measure the boundary-layer thickness, δ, at free-stream flow velocity $U = 8.2$ m/s. Here, δ is customarily defined as the distance from the wall to the point where $u(y) = 0.99\,U$, beyond which the flow velocity is essentially U. The measured δ was about 4.0 mm in the present case, corresponding to a uniform flow region in the duct from $y = -46$ mm to $y = 46$ mm in y direction. The Reynolds number was 5980 based on the thickness of bluff body and the free-stream velocity $U = 8.2$ m/s.

3. Parameter identification and control performance for various leading edges

3.1. Vibration characteristics and optimal control parameters

Firstly, the vibration characteristics of the vibrating plate on the test model, being excited by embedded THUNDER actuators, were investigated by measuring the displacement at the center of plate using a laser vibrometer. The results shown in Fig. 3 include two cases: (1) various controlled excitation frequencies at a constant control voltage of 160 V; (2) various control voltages at the optimal control frequency. It was observed from Fig. 3(a) that the test model's frequency

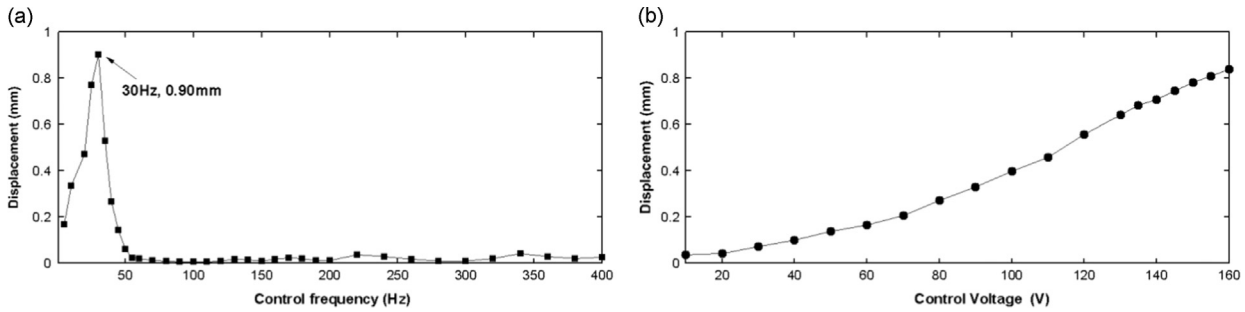

Fig. 3. Vibration characteristic of the vibrating plate on the test model, measured at the center of the vibrating plate. (a) At various control frequencies. The control voltage was set to 160 V; (b) At various control voltages. The control frequency was set to 30 Hz.

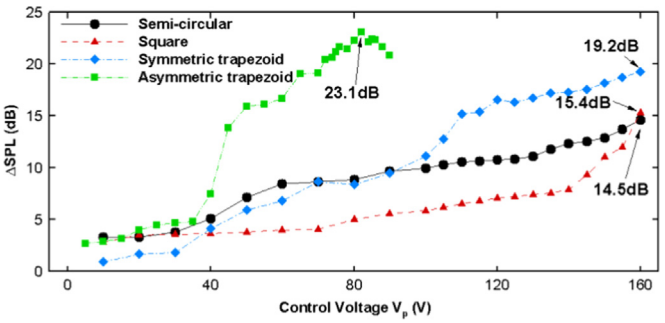

Fig. 4. The control performance for different control voltages at U=8.2 m/s for various leading edges of the test model, measured by microphone inside the duct. The control frequency was set to 30 Hz.

response peaked at around 30 Hz, and rapidly decreased in magnitude as the excitation frequency increased. The maximum displacement of control actuation of the test model was measured to be 0.90 mm at approximately 30 Hz. It is clear that a large actuation of the test model would be better for achieving a satisfactory control performance. Therefore, the optimal control frequency was chosen to be 30 Hz. Fig. 3(b) shows that at the optimal control frequency 30 Hz, the displacement d_p of the vibrating plate installed on the upper surface of the test model monotonously increased with the increase of control voltage.

The developed control system [20] was implemented to the system to control the vortex shedding and the flow-induced noise in the duct. As concluded those papers, the THUNDER actuators had an optimum activation frequency. Therefore, the amplitude of the control voltage was to be adjusted. The effect of varying the control voltage at 30 Hz on the noise reduction in the duct is shown in Fig. 4 in terms of Sound Pressure Level reduction (ΔSPL) with respect to their uncontrolled counterparts for four different leading edges. Here, ΔSPL is the magnitude difference between the peaks of the noise spectra at the vortex shedding frequency before and after the active control was implemented. The control voltage was about 160 V, which was limited by the maximum voltage allowable for THUNDER actuators, the control voltage could not be further increased, since high control voltage might damage the THUNDER actuators. A microphone installed in the duct recorded the same general trend of increasing noise reduction as the control voltage was increased for these four different leading edges, while for the asymmetrical configuration, it was found that a further increase of control voltage ($V_p > 82$ V) would not result in a better performance.

Furthermore, for the square leading edge test model, a gradual noise reduction was observed as control voltage was increased from 0 to 130 V. However, a significant increase in noise reduction level was observed when the control voltage $V_p > 130$ V. Since the displacement of the vibrating plate at the test model has a gradual increase with the increase of control voltage (as shown in Fig. 3(b)), the drastic change in the noise reduction level should not be attributed to the sudden change of control action. It is known that the vortex shedding generated behind the square leading edge test model could be described by the 'leading edge vortex shedding' (LEVS) [24,25], which began at the leading edge and then travelled downstream along a horizontal parabolic path. It was observed that when the fluid flows pass a leading or trailing edge of the test model, a shear or velocity gradient would exist in a layer of fluid flow, this layer of fluid flow was called 'shear layer' [24,25]. The region of shear layer with increasing amplitudes close to the surface of square leading edge test model was stronger than those for the semi-circular and symmetric trapezoid leading edge models, as will be observed in the measurements described in Section 4.1. Based on the observation, one plausible reason is that when control voltage $V_p > 130$ V and displacement $d_p > 0.64$ mm, the vibrating plate generated a large enough perturbation to influence the shear layer, leading to a significant weakening of the vortex shedding as shown in Fig. 4.

Furthermore, a special phenomenon was observed for the asymmetric trapezoid leading edge test model. The vortex shedding is generally generated downstream the test model through the interaction between the two separating shear layers on both sides of the bluff body [24,25]. For the asymmetric trapezoid leading edge test model, as observed in the measurement, the vortex shedding was mainly generated on the upper surface of test model and propagated downstream for a short distance, as will be observed in the measurements described in Section 4.1. In Fig. 4, the best control performance can be achieved at relatively low control voltage of around 82 V. In summary, the surface perturbation technique seems to be effective for all four typical leading edges.

It should be noted that the vortex shedding frequency is not of a multiple integer of 30 Hz, which is the control frequency used. The present experiments indicate this complex fluid–structure interaction affects the higher harmonics of the vortex shedding frequency that cause the noise reductions at higher harmonics. Thus, different control frequencies can be used as long as they can provide sufficient level of maximum displacement for the control actuation, since the control performance is mainly affected by the magnitude of surface perturbation.

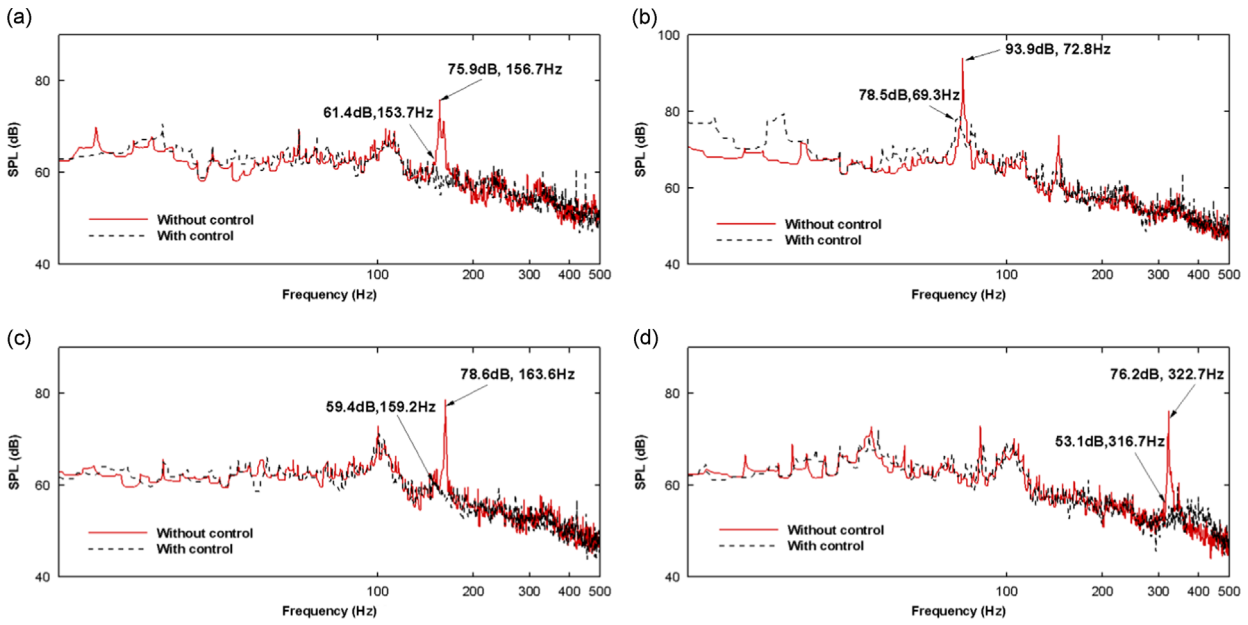

Fig. 5. Control performance shown in frequency-domain at $U=8.2$ m/s, measured by microphone inside the duct. The control frequency was 30 Hz. (a) Semi-circular leading edge test model; (b) Square leading edge test model; (c) Symmetric trapezoid leading edge test model; (d) Asymmetric trapezoid leading edge test model. The corresponding control voltages are 160 V, 160 V, 160 V and 82 V, respectively.

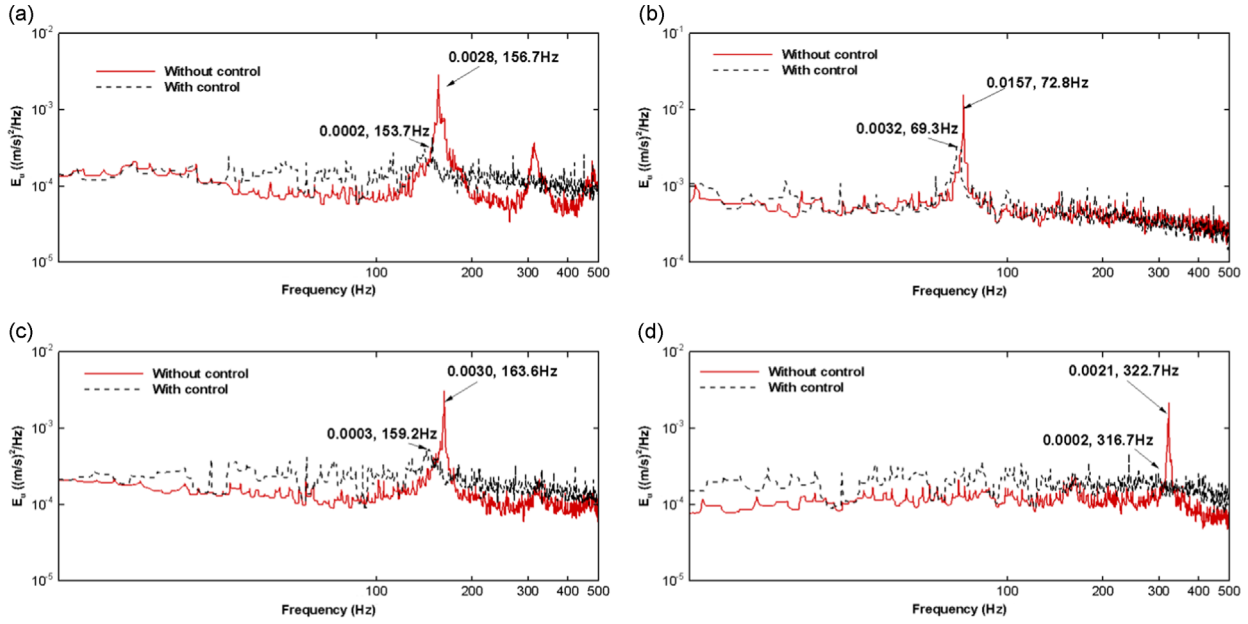

Fig. 6. Control performance shown in frequency-domain at $U=8.2$ m/s, measured by hot wire at $x=34$ mm, $y=11$ mm. The control frequency was 30 Hz. (a) Semi-circular leading edge test model; (b) Square leading edge test model; (c) Symmetric trapezoid leading edge test model; (d) Asymmetric trapezoid leading edge test model. The corresponding control voltages are 160 V, 160 V, 160 V and 82 V, respectively.

3.2. Control performance

Using the optimal control voltage obtained in the previous analysis, the control performance was further investigated in both sound and flow fields. Fig. 5 depicts the sound pressure spectra obtained from the Fast Fourier Transform (FFT) of time domain signals from respective microphone's measurements inside the duct for four different leading edges, with a frequency resolution of 0.1 Hz. It can be seen that, upon control deployment, the sound pressure in the duct underwent significant reductions for all cases. The spectra indicated that with control, the SPL in the duct decreased from 75.9 dB to 61.4 dB (a reduction of 14.5 dB), 93.9 dB to 78.5 dB (a reduction of 15.4 dB), 78.6 dB to 59.4 dB (a reduction of 19.2 dB) and

76.2 dB to 53.1 dB (a reduction of 23.1 dB) for the respective semi-circular, square, symmetric and asymmetric trapezoid leading edges at the vortex shedding frequency. Furthermore, it was found that there was a moderate increase in noise level at low frequencies when control was applied on the system, as shown in Fig. 5. This extra noise was generated by the fluid–structure interaction between the upper surface of the vibration plate and the flow field around the test model at the optimal control frequency.

The control effect in the flow field was investigated in terms of the power spectrum density of flow velocity E_u measured by hot wire, located at downstream of the test model at $x=34$ mm, $y=11$ mm ($x=29.5$ mm, $y=11$ mm for the square leading edge test model), as shown in Fig. 6(a–d). Here, E_u is the power spectrum density of the measured velocity flow fluctuation with the unit $(m/s)^2/Hz$. From the figures, it can be seen that E_u at the vortex shedding frequency has decreased from 2.8*e*-3 to 2.0*e*-4 (a reduction about 92.8%), 1.5*e*-2 to 3.2*e*-3 (a reduction about 80.0%), 3.0*e*-3 to 3.0*e*-4 (a reduction about 90.0%) and 2.1*e*-3 to 2.0*e*-4 (a reduction about 90.5%) for the respective semi-circular, square, symmetric and asymmetric trapezoid leading edges at the vortex shedding frequency. Though the hot wire could only measure the flow velocity fluctuations, these velocity fluctuations were indicative of the vortex shedding, with the strength reduction of the velocity fluctuations indicated the corresponding reduction on the vortex shedding. Therefore, the control was also effective in reducing the flow velocity levels generated by the vortex shedding. Moreover, although the location of vortex center was not known exactly, it was observed from the streamwise and lateral measurements (shown as the Figs. 8 and 10 in Section 4) that there was a consistent reduction of peaks in the power spectrum after the control application. It could thus be inferred that there had been reduction in the strength of vortex shedding because of the control action. Therefore, the hotwire measurement results can be reliably used to identify the strength of the vortex shedding.

Furthermore, it was found that for all these cases the vortex shedding frequencies were shifted to a lower value after the surface perturbation application. This observation agrees with the previous results [20,21], and the detail for this phenomenon will be explained in Section 4.2. An interesting observation is the appearance of dominant sub-harmonics and higher-order harmonics of vortex shedding frequency, indicating the non-linear nature of the system of interest. It is generally known that the vortex shedding frequency can be determined by the distance between the two shear layers behind a test model [1]. The test models used in this work have the same thickness, but the distance of the shear layers will be slightly different due to variation in leading edge types, leading to a slightly different fundamental vortex shedding frequency. For the asymmetric trapezoid leading edge test model, the second harmonics of vortex shedding frequency is the dominant harmonics at 322.7 Hz. For the square leading edge test model, the first sub-harmonics at 72.8 Hz dominated the system response.

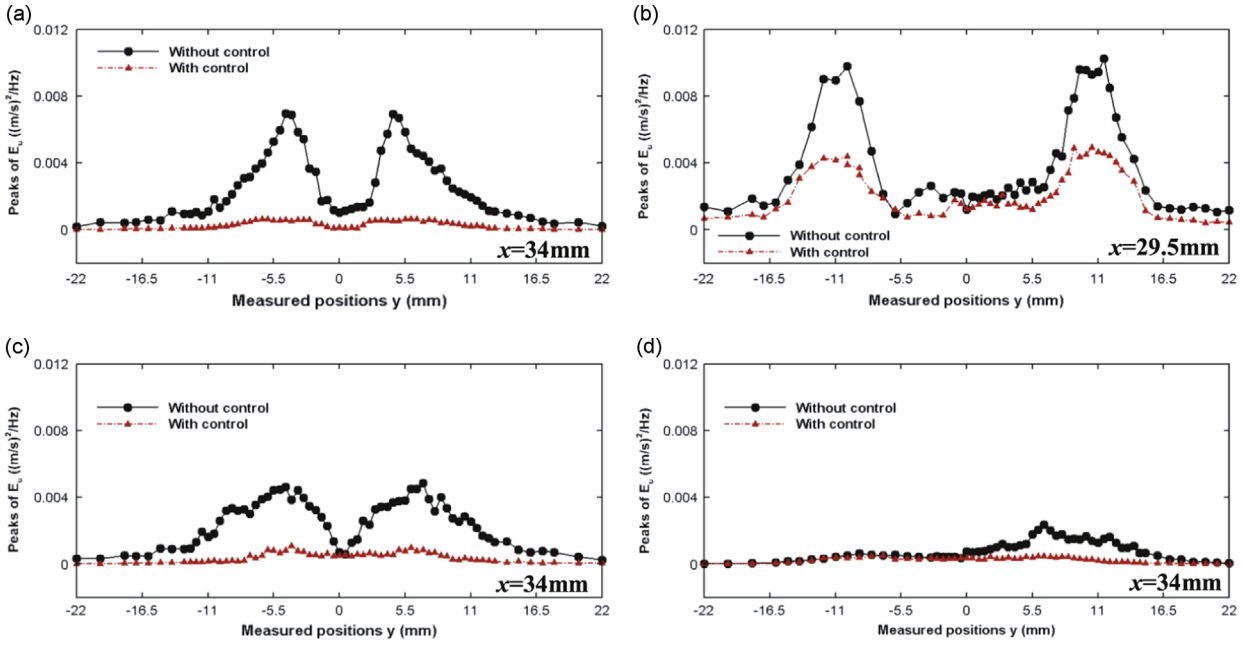

Fig. 7. The comparison of the peak values of E_u between before and after control for measured by hot wire along the path y axis from -22 mm to 22 mm behind the test model at $U=8.2$ m/s. (a) Semi-circular leading edge test model; (b) Square leading edge test model; (c) Symmetric trapezoid leading edge test model; (d) Asymmetric trapezoid leading edge test model.

4. Discussions on the control mechanisms

4.1. The vortex shedding strength reduction mechanisms of various leading edges

Experiments were performed to examine the vortex shedding type around various leading edge test models. A hot wire was moved along the y-direction at $x=34$ mm ($x=29.5$ mm for the square leading edge test model). The power spectrum density of flow velocity E_u at the vortex shedding frequency was measured before and after control, with results shown in Fig. 7. For the symmetric leading edge test models, a relatively symmetric power spectrum density distribution can be observed. For these cases, there are two maximum peak values within the range $y=-22$ mm to $y=22$ mm. These maximum peaks can be attributed to the strongest shear layer, which are the regions of flows with significant velocity gradient [26] associated with the shear layer. The interaction of two shear layers on both sides of bluff body can subsequently generate the vortex shedding that propagates downstream [1]. If the shear layers on both sides of test model do not have the same strength due to the non-symmetric surfaces or other conditions, the stronger shear layer will dominate the interactions between these two shear layers, leading to asymmetric power spectrum density distributions behind the test model. In general, the vortex shedding behind the semi-circular test model is called the trailing edge vortex shedding (TEVS), while the vortex shedding behind the square leading edge is called the leading edge vortex shedding (LEVS) [24,25,27,28]. The characteristic of these TEVS and LEVS can be observed in Fig. 7. It is found that the maximum strength of TEVS occurred at approximately $y=-5.5$ mm and $y=5.5$ mm, which correspond to the upper and lower sides of semi-circular leading edge test model shown in Fig. 7(a). For the square leading test model result shown in Fig. 7(b), however, the maximum strength of LEVS occurred at approximately $y=-11$ mm and $y=11$ mm, which were located further upper and lower than those for the semi-circular leading edge test model. The width of shear layers for the symmetric and asymmetric trapezoid leading edge test models, shown in Fig. 8(c-d), are wider than that of shear layers for individual TEVS and LEVS cases. These results were confirmed by Deniz and Staublib [27] who showed that the flow for the symmetric trapezoid leading edge test models is separated at the leading-edge, but the leading-edge vortices are at the side surfaces and/or edges of the body before separating from the trailing edge. Thus the vortex shedding behind these types of bluff bodies should be the intermediate case between the TEVS and LEVS. Here the intermediate means the shear layer observed behind the bluff body contains the characteristics of shear layers that represent both TEVS and LEVS. This is based on the observation of the shear layer measured for separate TEVS (the semi-circular leading edge) and LEVS (the square leading edge) cases, as shown in Fig. 7. Similar results were observed by Taylor et al. [28] who used the test models with the square, semi-circular and triangular leading edges to study the features of vortex shedding around the bluff bodies. It was observed that the corresponding vortex shedding types for those test models were respectively LEVS, TEVS and the intermediate case between the TEVS and LEVS.

For further investigation, the power spectrum density distribution was also measured by using a hot wire that was moved along x direction at $y=11$ mm. The peak values E_u at the vortex shedding frequency were then measured before and

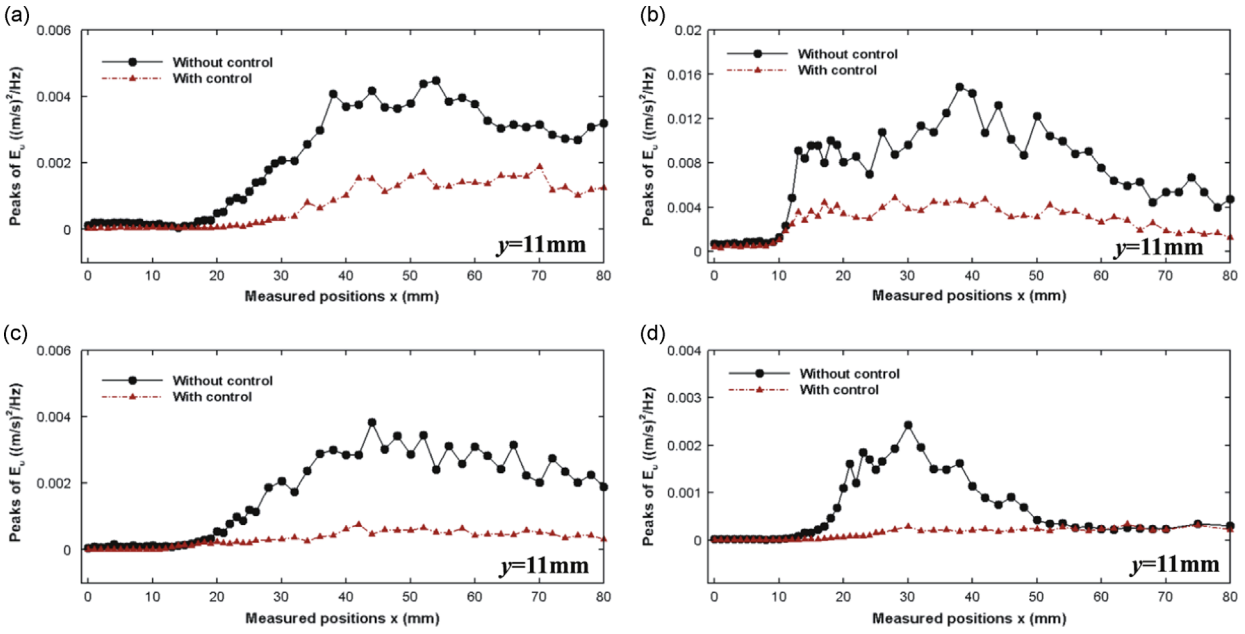

Fig. 8. The comparison between without control and with control for the peak values of E_u measured by hot wire along the path $y=11$ mm, x from 0 to 80 mm at $U=8.2$ m/s. (a) Semi-circular leading edge test model; (b) Square leading edge test model; (c) Symmetric trapezoid leading edge test model; (d) Asymmetric trapezoid leading edge test model.

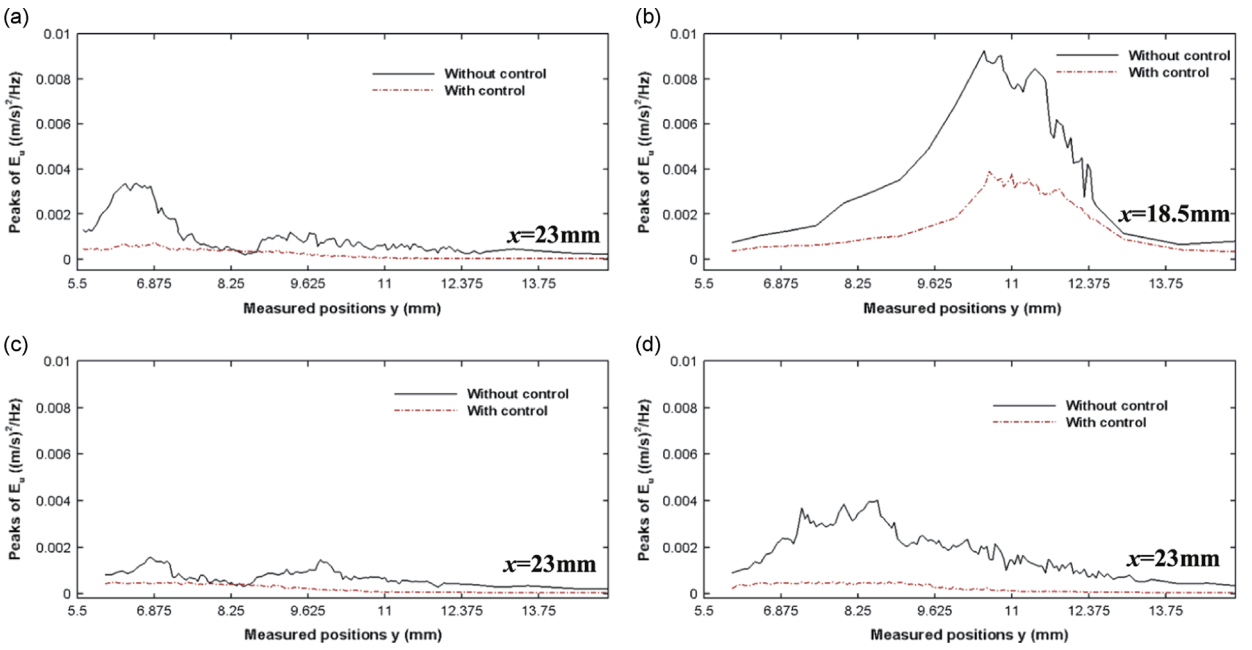

Fig. 9. The comparison of the peak values of E_u between before and after control for measured by hot wire along the path y axis from 5.6 mm to 15.0 mm on the trailing edge the test model at U=8.2 m/s. (a) Semi-circular leading edge test model; (b) Square leading edge test model; (c) Symmetric trapezoid leading edge test model; (d) Asymmetric trapezoid leading edge test model.

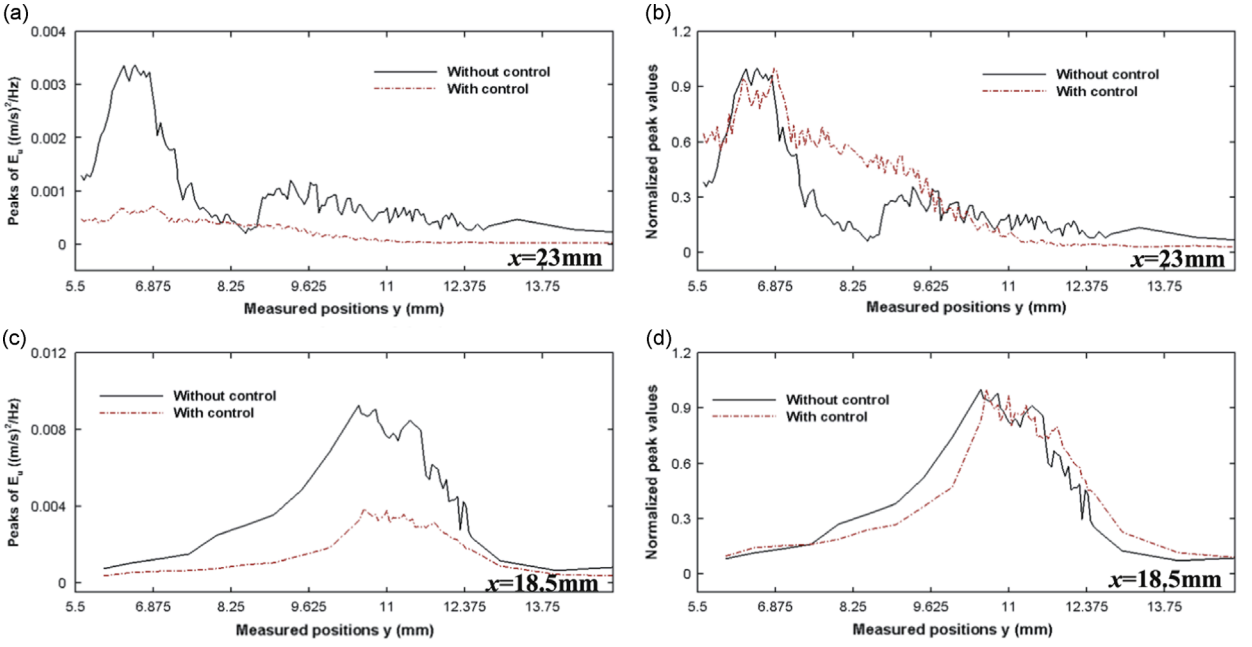

Fig. 10. The shear layer shift phenomenon, measured by hotwire along the trailing edge of the test model at U=8.2 m/s. (a) Measured peak values for y from 6.00 mm to 15.00 mm behind the square leading edge test model; (b) Normalized peak values for y from 6.00 mm to 15.00 mm behind the square leading edge test model; (c) Measured peak values for y from 5.60 mm to 15.00 mm behind the semi-circular leading edge test model; (d) Normalized peak values for y from 5.60 mm to 15.00 mm behind the semi-circular leading edge test model.

after control as shown in Fig. 8. From Fig. 8(a), the shear layer strength associated with TEVS, slowly increased from the trailing edge until they reached the more stable state at x=40 mm downstream the test model. For the LEVS case shown in Fig. 8(b), vortex shedding has already started upstream the trailing edge, which agrees with the experimental results done by Stokes and Welsh [25], which stated that for the short bluff body, the vortex shedding is generated by the interaction of two shear layers behind a test model. However, for the case of asymmetric trapezoid leading edge test model in Fig. 8(d),

there was no stable vortex shedding occurring downstream the test model. The plausible reason is that the two shear layers on both sides of test model were not similar as indicated in Fig. 7(d). As a result, unequal shear layers could not develop into stable vortex shedding, and these shear layers would dissipate after only a short distance behind the test model. This observation demonstrates that a surface perturbation control technique can be used to create unbalanced shear layers, by simply generating the surface perturbation on one side of test model.

A hot wire was moved from $y=6.00$ mm to 15.00 mm (from $y=5.60$ mm to 15.00 mm for the semi-circular leading edge test model) at the trailing edge of the test models for measuring the power spectrum density of flow velocity E_u at the vortex shedding frequency before and after control, as shown in Fig. 9.

It can be observed from Fig. 9(a) that the maximum peaks of E_u are located around $y=6.50$ mm for the semi-circular leading edge test model, which is consistent to the corresponding maximum peaks at around $y=5.50$ m in Fig. 7(a). The locations of the maximum peaks are different between the two figures because of different flow structures at the measured positions. The results in Fig. 9(a) were measured at the trailing edge of the test model, while results shown in Fig. 7(a) were measured at $x=34$ mm from Fig. 9(a), the maximum peaks of E_u should be away from the surface of the test model, since the generated vortex shedding behind the test model was attracted by the other shear layer at the opposite surface of test model, causing the maximum peaks of E_u to be shifted closer to the lower surface. These results are agree with the descriptions in Gerrard's paper [1]. After applying control action, these maximum peaks were reduced to smaller values as shown in Fig. 9(a), as the corresponding maximum peaks also suppressed in Fig. 7(a). Similar comparisons can also be found in Fig. 10(b–d) and Fig. 8(b–d). It is clear that the surface perturbation applied between the leading edge and the trailing edge, can affect the downstream flow structures or the vortex shedding.

For the symmetric trapezoid and asymmetric trapezoid leading edge test models, the flow structures at the trailing edges are quite different from each other as shown in Fig. 9(c) and (d). The maximum peaks of E_u for the symmetric trapezoid leading edge are located at around $y=6.5$ mm and $y=9.6$ mm, while for the asymmetric trapezoid leading edge, the maximum peak is at around $y=8.2$ mm. The asymmetric trapezoid leading edge test model, however, does not have balanced shear layers as shown in Fig. 7(d), leading to no stable vortex shedding behind the test model. In contrast, the symmetric trapezoid leading edge test model has two symmetric shear layers behind the test model as shown in Fig. 7(c), therefore the interaction of shear layers generates the stable vortex shedding which propagates downstream. Since the trapezoid leading edge is the intermediate case between the semi-circular and square leading edges, the vortex shedding behind the bluff body is not simply the TEVS or LEVS. Fig. 9(c) indicates that the combined aspect of TEVS and LEVS exists behind the trapezoid leading edge. Therefore, its physical mechanism can be regarded as the combination of the vortex shedding mechanisms for the semi-circular and square leading edge.

Based on the present experimental results, the vortex shedding mechanism can be generalized for more general types of leading edges, with special cases for the semi-circular leading edge with its TEVS, and the square leading edge with its LEVS. For trapezoid leading edges, it is observed that the vortex shedding mechanism is a combination of LEVS and TEVS. The incoming flows can be divided into two kinds of flows when passing over the trapezoid leading edge, some are still attached to the surface of the bluff body while the others are separating and they act as independent shear layers.

Another aspect worth investigating is for the asymmetric trapezoid leading edge test model. As shown in Fig. 7(d), there was rather weak vortex shedding at $y=6.5$ mm, compared to that associated with TEVS for semi-circular and symmetric trapezoid leading edges (Fig. 7(a) and (c)). However, due to instability of vortex shedding, the vortex shedding weakened downstream (see Fig. 8(d)). Fig. 8(d) shows that there still has vortex shedding near the trailing edge of the asymmetric trapezoid leading edge test model. However, the flow structures from the upper and lower surfaces of the test model cannot regularly interact with each other, so the vortex shedding disappear within a short distance behind the test model. Fig. 7(d) depicts this unbalanced vortex shedding, where the vortex shedding at above the bluff body ($y=6.5$ mm) is considerably stronger than that under it ($y=-6.5$). Furthermore, the maximum strength of vortex shedding occurred at about $y=6.5$ mm (See Fig. 7(d)) which is mainly caused by TEVS generated from the attached flow structures on the upper surface of test model, while the LEVS could not be generated effectively due to two different separating shear layers on the leading edge. Therefore the LEVS initially dominated TEVS at the trailing edge, but due to its instability the LEVS weakened downstream and TEVS started to dominate although at a weakened state. This phenomenon indicates that if the regular flow structures from the upper and lower surfaces can be disturbed using a surface perturbation, the interaction between the flow structures can be affected in a way that the vortex shedding generations can be suppressed. The results also indicate that apart from using an active control method, a passive control method by using an asymmetric surface on the bluff body can also be used to suppress the vortex shedding downstream.

Based on the investigation, the vortex shedding characteristics over a bluff body is affected by the relative strength of LEVS and TEVS. If the leading edge geometry is more squared, relatively strong LEVS will be generated that can dominate over TEVS since its shear layer develops earlier. If the leading edge geometry is more semi-circular, relatively weaker LEVS will be generated and TEVS will dominate as the consequence. In the case of the asymmetric leading edge, the stability of both LEVS and TEVS cannot be maintained, because there are no regular interactions of flow structures generated from both surfaces of bluff body. The applied surface perturbation between the leading edge and trailing edge generates additional vortices that interact with the vortex shedding process by altering the flow structure around the test model. These additional vortices from the oscillating vibration plate will destroy the spatial coherency of the trailing edge vortex system [20]. As the consequence, all these processes contribute to the reduction of the strength of shear layers, resulting in a reduction of vortex shedding downstream the test model. While for the free shear layers which are separating at the leading edge, the

shear layers gradually propagate away from the surface of the test model at the separate point, from $x=0$ mm, $y=\pm 5.5$ mm to the position of around $x=29.5$ mm, $y=\pm 11$ mm for the present cases. The applied surface perturbation can generate the required flow disturbance to weaken the shear layers, so weak vortex shedding is generated.

In addition, although the surface perturbation was applied only on one side of the various leading edge test models, the effect on the flow structure occurred on both sides of the test models, as evidenced by the symmetric feature of the curves shown in Fig. 7(c). This phenomenon can be explained by considering the formation mechanism of the vortex shedding. In fact, the vortex street is generated behind the test model through the interaction between the two separating shear layers on both sides of the bluff body. The one-sided perturbation disturbs one of the shear layers and subsequently alters its interaction with the other shear layer, leading to a reduction of the vortex shedding strength. Therefore, the proposed surface perturbation technique does not need to be applied on both surfaces of the bluff body for achieving satisfactory control performance.

In summary, the alteration on upstream flow structures could change the downstream flow structures by creating unbalanced shear layers. As a consequence, the vortex shedding strength can be affected leading to the reduction of flow-induced noise in the duct. The strength of the vortex shedding is determined by the relative strength and the distance of the shear layers. Therefore, one of key factors for controlling the vortex shedding behind the bluff bodies is by altering the shear layers to prevent the generation of vortex shedding [1]. It was observed from Figs. 8–10 that after the control application using surface perturbation, the flow structure around the test model was altered, thus the flow structure behind the test model was correspondingly changed. The strong shear layers behind the test model were reduced to relatively weak shear layers, resulting in the generation of weak vortex shedding. Fig. 8 shows that from the leading edge to the downstream of the test model, the vortex shedding have been suppressed after applying the surface perturbation control.

4.2. Shear layer shift mechanism

It is observed in Figs. 5 and 6 that the vortex shedding frequency was shifted to a lower value after applying the surface perturbation. Previous work [20] had concluded that the shift of the vortex shedding frequency can be attributed to the effect of the perturbation and it can be quantified in terms of displacement by using a simple formula. Furthermore, Gerrard [1] has pointed out that there are two important factors for determining the vortex shedding frequency behind bluff bodies: the distance between two shear layers and the turbulence of the shear layers. When the shear layers are brought closer together, the periodic time is shortened. An increase in the turbulence in the shear layers will result in their being more diffuse in the region of interaction and take longer for initiate shedding. In the present paper, more measurements were conducted to investigate the boundary layer or shear layer alteration at the trailing edge of the test model by using the hot wire. The results can be used to explain the physical mechanism of the vortex shedding frequency shift. Since the vortex shedding behind the symmetric trapezoid leading edge test model are the combination of TEVS and LEVS, while the asymmetric trapezoid leading edge test model does not have stable vortex shedding, the present analysis is only focused on the semi-circular and square leading edge test models.

Firstly, a hot wire was moved from $y=5.60$ mm to 15.00 mm at the trailing edge of the semi-circular leading edge test model, and the minimum step for measurement was $\Delta y=0.05$ mm. Values of E_u at the vortex shedding frequency were then measured before and after control with results shown in Fig. 10(a) for the semi-circular leading edge test model. In order to compare the power spectrum density distribution before and after control in the same scale, the normalized peaks of E_u before and after control at the vortex shedding frequency, were plotted in Fig. 10(b) for the semi-circular leading edge test model. To evaluate the shifting of shear layers, a measure is introduced by using the centroid or the geometric center of the area under each curve. For the analysis, the bandwidth is chosen to be the region with relatively high shear layer strength from $y=5.60$ mm to 7.80 mm as shown in Fig. 10(b). Based on the measurement data, the centroid's y-location is found to be 6.59 mm for the case without control. It is noted in Fig. 5(a) that the surface perturbation has shifted the vortex shedding frequency from 156.7 Hz to 153.7 Hz, a frequency shift of about 3.0 Hz. Using the equation developed in previous work [20], it is predicted that the overall increase of effective displacement between two shear layers is about 0.21 mm, indicating that the shift for each shear layer is about 0.105 mm. After applying the surface perturbation, the original shear layers were disturbed to a relatively weaker shear layer. Based on measurement data shown in Fig. 10(b), it is found that the new centroid's y-location is 6.69 mm, reflecting a shift of 0.10 mm from the original shear layers to the new shear layer. The centroid's shift is indeed reasonably close to the predicted value of 0.105 mm, associated with the vortex shedding frequency shift of 3.0 Hz.

Secondly, a hot wire was moved from $y=6.00$ mm to 15.00 mm at the trailing edge of the square leading edge test model, and the minimum step for measurement was $\Delta y=0.05$ mm from $y=10.50$ mm to 12.50 mm. Values of E_u at the vortex shedding frequency were then measured before and after control with results shown in Fig. 10(c). In order to compare the power spectrum density distribution before and after control in the same scale, the normalized peaks of E_u before and after control at the vortex shedding frequency, were plotted in Fig. 10(d). The bandwidth of the calculation for the centroid is chosen to be the region with relatively high shear layer strength from $y=9.00$ mm to 13.00 mm as shown in Fig. 10(d). Based on the measurement data, the centroid's y-location is found to be 10.82 mm for the case without control. It is noted in Fig. 5(b) that the surface perturbation has shifted the vortex shedding frequency from 72.8 Hz to 69.3 Hz, a frequency shift of about 3.5 Hz. Using the equation developed in previous work [20], it is predicted that the overall increase of effective displacement between two shear layers is about 0.52 mm, indicating that the shift for each shear layer is about 0.26 mm.

After applying the surface perturbation, the original shear layers were disturbed to a relatively weaker shear layer. Based on measurement data shown in Fig. 10(d), it is found that the new centroid's y-location is $y=11.05$ mm, reflecting a shift of 0.23 mm from the original shear layer to the new shear layer. The centroid's shift is indeed reasonably close to the predicted value of 0.26 mm, associated with the vortex shedding frequency shift of 3.5 Hz.

The above observation confirms that the actively controlled perturbation actually generates a flow structure alteration on the upper surface of the test model. This control action does not only weaken the shear layers, but also separates the two shear layers away from each other same as observed by the hot wire measurements. As a result, the overall increase of effective displacement between shear layers leads to a shift in the vortex shedding frequency.

4.3. *Effective perturbation position for various leading edges*

The previous experiment utilized a vibration plate that almost covered the entire upper surface of test model. In practice, only a part of the surface on the test model may be used for surface perturbation. So the effective surface perturbation positions for both the square and semi-circular leading edges need to be carefully investigated. Such an investigation will provide insights into how an optimal control strategy can be implemented for test models with different leading edges.

The test model with the reduced surface area was developed to investigate the effect of surface perturbation location to the control performance. For the design of the test model, the width of the vibration plate should be as small as practically possible to allow the surface perturbation to be generated at a specific point-wise location over the test model. This assists with the analysis since the surface perturbation could be applied at this point-wise location. For this purpose, a suitable dimension for the vibration plate was carefully considered due to the fabrication limitation. The use of vibration plate with different widths (1 mm, 2 mm and 3 mm) has been investigated and it was found that that the one with 3 mm width provide the most practical option for the test model, allowing the vibration plate to have only 13% coverage out of the total surface area of the test model. The locations for the vibration place were deliberately chosen nearby the leading edge and trailing edge respectively, to investigate the effect of surface perturbation in influencing the leading edge vortex shedding or trailing edge vortex shedding for a number of test model configurations. Thus a 3 mm-vibration-plate was installed on the upper surface of the test models, including the semi-circular leading edge and square leading edge test model. As shown in Fig. 11(a), the 3 mm-vibration-plate was installed 6 mm away from the semi-circular leading edge, but 14mm away from the trailing edge, and it was classified as C-1 test model. In Fig. 11(b), the 3 mm-vibration-plate was installed 1 mm away from the trailing edge but 19 mm away from the semi-circular leading edge and it was classified as C-2 test model. These two positions shown in Fig. 11(a) and (b) are the two important positions in the vortex generation region which are related to the initial stability of shear layer and the generation of the TEVS. In Fig. 11(c) and (d), the 3 mm-vibration-plate was installed 1mm away from the square leading edge, but 15 mm away from the trailing edge, and it was classified as S-1 test model.

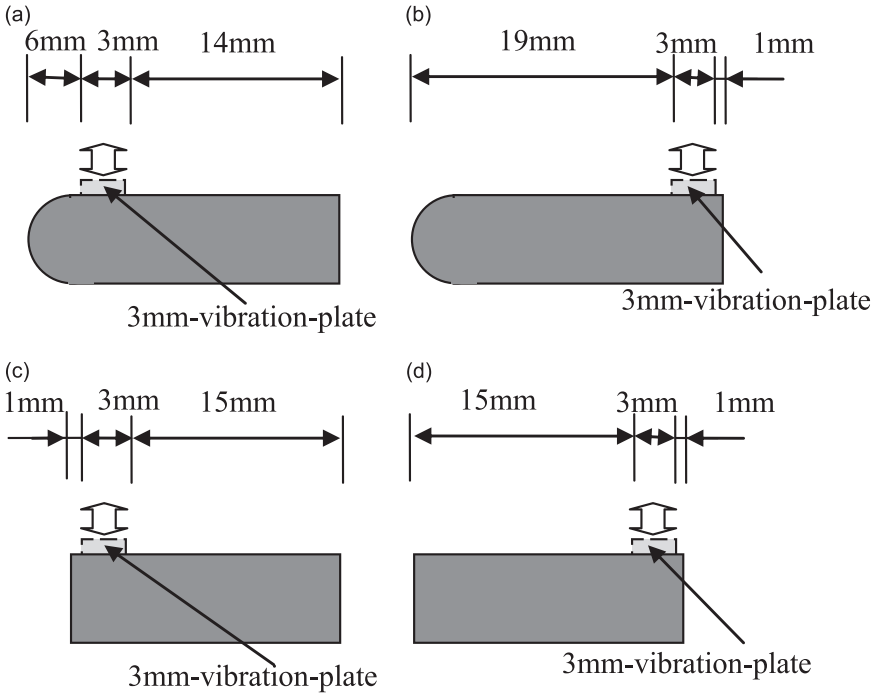

Fig. 11. The sketch for the 3 mm-vibration-plate semi-circular and square leading edge test model. (a) C-1; (b) C-2; (c) S-1; (d) S-2.

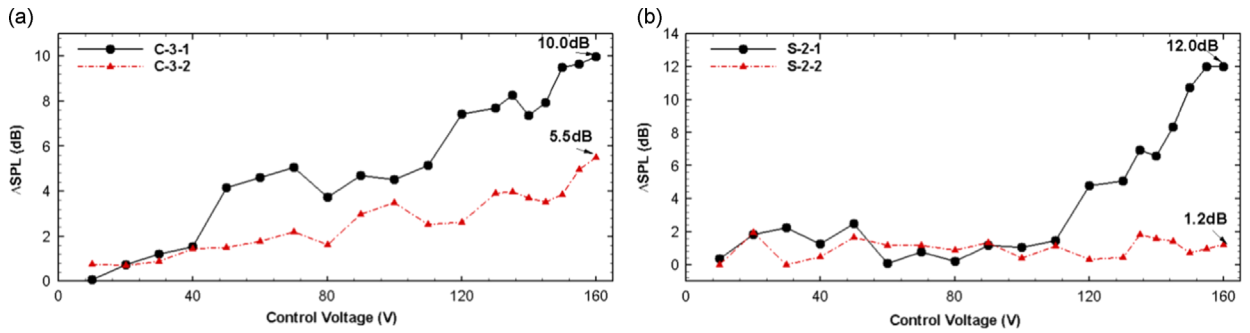

Fig. 12. The control performance of different perturbation positions at U=8.2 m/s. (a) Semi-circular leading edge test model; (b) Square leading edge test model.

Finally, the 3 mm-vibration-plate was installed 1mm away from the trailing edge but 15 mm away from the square leading edge, classified as S-2 test model.

Various measurements were conducted by using the surface perturbation. The noise reductions measured in the duct by increasing the control voltages are shown in Fig. 12(a) for the semi-circular leading edge test model. It was found that the control action applied at these two positions were both effective in reducing the noise in the duct. The best control performances of 10.0 dB for the case of C-1 and 5.5 dB for the case of C-2 were achieved. From the results, it is clear that the control performance for the case when the perturbation was near the leading edge is better than the case that the perturbation position was near the trailing edge. Therefore, it is beneficial to locate the surface perturbation near the semi-circular leading edge. This result is expected because the additional vortices generated by this surface perturbation can develop further downstream so to be able to affect the TEVS in a more effective way. Although the surface perturbation only covered 13% of the upper surface of test model, the configuration can be used to achieve 10 dB SPL reduction in the duct. This is compared to 14.5 dB SPL reduction achieved using the surface perturbation that covered 100% of the upper surface.

For the square leading edge test model, the best control performance of 12.0 dB for the case of S-1 and 1.2 dB for the case S-2 were achieved (Fig. 12(b)). The control was only effective when the perturbation was applied near the leading edge of the test model. When the perturbation was applied near the trailing edge, the vortex shedding had already fully developed and stable at some distance away from the surface of the test model. The small surface perturbation generated by the vibration plate in the study could not directly affect the vortex shedding but influenced it via the vertical velocity generated by the vibration plate. The vertical velocity was much smaller than flow velocity contained in the vortex shedding, so the vertical velocity perturbation could only disturb the vortex shedding strength by a small amount. When the surface perturbation technique was applied near the leading edge of the test model, the surface perturbation could better influence the path of LEVS. Using only 13% of the vibration surface, such a control configuration could achieve a 12 dB SPL reduction measured in the duct, in contrast to a 15.4 dB SPL reduction using 100% of vibration surface. Contrasting the results for both leading edges, it can be observed that better noise reduction was achieved by the semi-circular leading edge when the vibration surface was located near the leading edge. This can be expected since the surface perturbation can be applied upstream the generated vortex shedding for the semi-circular leading edge, while the perturbation can only be applied downstream the vortex shedding for the square leading edge.

In summary, although the effective perturbation positions for semi-circular and square leading edges are both located near the leading edge of the test models, the control strategies are completely different due to the different vortex characteristics of these two leading edges. For a square leading edge test model, the control action of the surface perturbation mainly takes effect in the vortex generation region. Although the surface perturbation can be located anywhere within this region, the optimal control strategy is to arrange the perturbation at the position near the leading edge where the shear layer is at its initial stage of development. By this way, an effective vortex strength and noise reduction can be achieved simply by using a narrow vibration plate and a low control voltage.

5. Conclusions

The surface perturbation technique was experimentally investigated for test models with various leading edges. Four leading edges were used since they represent typical leading edges commonly used in engineering applications. In the experiments, different size of the plate, chord length and the flow velocity had been tested, and the results shown in this manuscript were the primary results based on the experimental measurements and analysis. The main conclusions are summarized as follows:

(1) The surface perturbation was successfully applied for the flow-induced noise behind bluff bodies with various leading edges. With control, the SPL in the duct decreased from 75.9 dB to 61.4 dB (a reduction of 14.5 dB), 93.9 dB to 78.5 dB (a reduction of 15.4 dB), 78.6 dB to 59.4 dB (a reduction of 19.2 dB) and 76.2 dB to 53.1 dB (a reduction of 23.1 dB) for the

respective semi-circular, square, symmetric and asymmetric trapezoid leading edges at the vortex shedding frequency, which indicated that the vortex shedding and its flow-induced noise have been successfully suppressed. The control performance for a bluff body with a general leading edge can be explained by understanding the vortex shedding mechanism that is a combination of LEVS and TEVS.

(2) The surface perturbation between leading edge and trailing edge causes additional vortices that interact with the vortex shedding process by altering the flow structure around it, resulting in a reduction of the vortex shedding strength downstream the test model. On the other hand, the applied surface perturbation between the leading and trailing edge could generate the flow disturbance to weaken the shear layers developed early at the leading edge, leading to weaker vortex shedding downstream the test model. Additional, the investigation leads to a conclusion that the proposed surface perturbation technique does not need to be applied on both surfaces of a bluff body, since a one-sided surface perturbation should be sufficient for achieving satisfactory control performance.

(3) The surface perturbation alters the flow structure on the upper surface of the test models with various leading edges. This control action does not only weaken the shear layers, but also separates the two shear layers away from each other, resulting in a shift in the vortex shedding frequency. This phenomenon turns out to be critical in off-setting the acoustic resonance observed previously [20].

(4) The optimal control strategy is to arrange the perturbation at the position near the leading edge so that the surface perturbation can generate additional vorticities that can further develop in strength downstream. This way, an effective vortex strength and noise reduction can be achieved simply by using a narrow vibration plate and a low control voltage. Furthermore, the size of the vibration surface also matters since a larger surface perturbation can perturb a larger section of flow over the test model, generating more effective vortices for control purposes. For a given size of vibration plate, a lower control voltage can be achieved for the semi-circular leading edge test model since the perturbation can be applied before the vortex shedding is generated at the trailing edge.

Acknowledgements

The second author wishes to acknowledge the support provided by Ningbo Science and Technology Bureau – Technology Innovation Team (2011B81006), China.

References

[1] J.H. Gerrard, The mechanics of the formation region of vortices behind bluff bodies, *Journal of Fluid and Mechanics* 25 (1966) 401–413.
[2] P.M. Radavich, A. Selamet, J.M. Novak, A computational approach for flow-acoustic coupling in closed side branches, *Journal of Acoustical Society of America* 109 (2001) 1343–1353.
[3] N.B. Roozen, M. Bockholts, V.E. Pascal, A. Hirschberg, Vortex sound in bass-reflex ports of loudspeakers. Part I. Observation of response to harmonic excitation and remedial measures, *Journal of Acoustical Society of America* 104 (1998) 1914–1918.
[4] L. Cattafesta, D. Williams, C. Rowley, F. Alvi, Review of active control of flow-induced cavity resonance, *AIAA Paper* (2003) 2003–3567.
[5] W.C.L. Shih, C. Wang, D. Coles, A. Roshko, Experiments on flow past rough circular cylinders at large Reynolds numbers, *Journal of Wind and Industrial Aerodynamics Engineering* 49 (1993) 351–368.
[6] E. Anderson, A. Szewczyk, Effects of a splitter plate on the near wake of a circular cylinder in 2 and 3-dimensional flow configurations, *Experiments in Fluids* 23 (1997) 161–174.
[7] C. Dalton, Y. Xu, J.C. Owen, The suppression of lift on a circular cylinder due to vortex shedding at moderate Reynolds numbers, *Journal of Fluids and Structures* 15 (2001) 617–628.
[8] S. Baek, H.J. Sung, Numerical simulation of the flow behind a rotary oscillating circular cylinder, *Physics of Fluids* 10 (1998) 869–876.
[9] S. Choi, H. Choi, S. Kang, Characteristics of flow over a rotationally oscillating cylinder at low Reynolds number, *Physics of Fluids* 14 (2002) 2767–2777.
[10] O. Cetiner, D. Rockwell, Streamwise oscillations of a cylinder in a steady current. Part 1: locked-on states of vortex formation and loading, *Journal of Fluid and Mechanics* 427 (2001) 1–28.
[11] H. Blackburn, R. Henderson, A study of two-dimensional flow past an oscillating cylinder, *Journal of Fluid and Mechanics* 385 (1999) 255–286.
[12] E. Berger, Suppression of vortex shedding and turbulence behind oscillating cylinders, *Physics of Fluids* 10 (1967) 191–193.
[13] X.Y. Huang, D.S. Weaver, On the active control of shear layer oscillations across a cavity in the presence of pipeline acoustic resonance, *Journal of Fluids and Structures* 5 (1991) 207–219.
[14] L.N. Cattafesta, S. Garg, M. Choudhari, F. Li, Active control of flow-induced cavity resonance, *AIAA Paper* (1997) 97–1804.
[15] L.N. Cattafesta, S. Garg, D. Shukla, The development of piezoelectric actuators for active flow control, *AIAA Journal* 39 (2001) 1562–1568.
[16] L.N. Cattafesta, J. Mathew, A. Kurdila, Modeling and design of piezoelectric actuators for fluid flow control, SAE Technical Paper 2000-01-5534, 2000.
[17] L. Cheng, Y. Zhou, M.M. Zhang, Perturbed interaction between vortex shedding and induced vibration, *Journal of Fluids and Structures* 17 (2003) 887–901.
[18] L. Cheng, Y. Zhou, Surface perturbation technique for flow-induced vibration and noise control, *Journal of Sound and Vibration* 310 (2008) 527–540.
[19] M.M. Zhang, L. Cheng, Y. Zhou, Asynchronous control of flow-induced acoustic cavity resonance using imbedded piezo-electric actuators, *Journal of Acoustical Society of America* 126 (2009) 36–45.
[20] Z.B. Lu, L. Cheng, Active control of flow-induced acoustic resonance through surface perturbation, *AIAA Journal* 50 (2012) 2566–2573.
[21] Z.B. Lu, D. Halim, L. Cheng, Closed-loop control of flow-induced sound in a flow duct with downstream resonant cavities, *Journal of Acoustical Society of America* 133 (2013) 1468–1479.
[22] V. Strouhal, Uber eine besondere Art der Tonerregung, *Annalen der Physik und Chemie* 5 (1878) 216–251.
[23] M.S. Howe, Contributions to the theory of aerodynamic sound, with application to excess Jet noise and the theory of the flute, *Journal of Fluid and Mechanics* 71 (1975) 625. -613.
[24] M.C. Welsh, A.N. Stokes, R. Parker, Flow-resonant sound interaction in a duct containing a plate, Part I: semi-circular leading edge, *Journal of sound and vibration* 95 (1984) 305–323.
[25] A.N. Stokes, M.C. Welsh, Sound interaction in a duct containing a plate, Part II: square leading edge, *Journal of sound and vibration* 104 (1986) 55–73.

[26] Piquet Jean, *Turbulent Flows: Models and Physics*, Springer, Germany, 1999.
[27] S. Deniza, T.H. Staublib, Oscillating rectangular and octagonal profiles: interaction of leading- and trailing-edge vortex formation, *Journal of Fluids and Structures* 11 (1997) 3–31.
[28] Z.J. Taylor, E. Palombi, R. Gurka, G.A. Kopp, Features of the turbulent flow around symmetric elongated bluff bodies, *Journal of Fluids and Structures* 27 (2011) 250–265.